THE JOURNAL OF PHYSICAL CHEMISTRY B

Article

pubs.acs.org/JPCB

Graphitic Carbon−Water Nonbonded Interaction Parameters

Yanbin Wu and N. R. Aluru*

Department of Mechanical Science and Engineering, Beckman Institute for Advanced Science and Technology, University of Illinois at Urbana−Champaign, Urbana, Illinois 61801, United States

ABSTRACT: In this study, we develop graphitic carbon−water nonbonded interaction parameters entirely from ab initio calculation data of interaction energies between graphene and a single water molecule. First, we employ the Møller−Plesset perturbation theory of the second order (MP2) method to compute the polycyclic aromatic hydrocarbon (PAH)−water interaction energies, with proper size of basis sets and energy component analysis to extrapolate to infinite-sized graphene limit. Then, we develop graphitic carbon−water interaction parameters based on the MP2 data from this work and the ab initio data available in the literature from other methods such as random-phase approximation (RPA), density functional theory-symmetry-adapted perturbation theory (DFT-SAPT), and coupled cluster treatment with single and double excitations and perturbative triples (CCSD(T)). The accuracy of the interaction parameters is evaluated by predicting water contact angle on graphite and carbon nanotube (CNT) radial breathing mode (RBM) frequency shift and comparing them with experimental data. The interaction parameters obtained from MP2 data predict the CNT RBM frequency shift that is in good agreement with experiments. The interaction parameters obtained from RPA and DFT-SAPT data predict the contact angles and the CNT RBM frequency shift that agree well with experiments. The interaction parameters obtained from CCSD(T) data underestimate the contact angles and overestimate the CNT RBM frequency shift probably due to the use of small basis sets in CCSD(T) calculations.

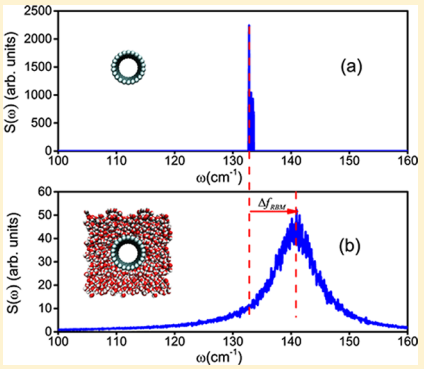

INTRODUCTION

Graphitic carbon based systems, for example, carbon nanotubes (CNTs), graphene, and graphite, have been investigated extensively for various applications, such as sensors mimicking biological systems,[1,2] nanochemical reaction chambers, and water filtration.[3,4] Various applications of graphene/CNTs require understanding of the graphitic carbon−water interaction. Molecular dynamics (MD) simulation has been a well-established tool to study water behavior in graphitic carbon based systems, for example, carbon nanotubes (CNTs), graphene, and graphite.[5−8] It has been shown that predicted properties using MD depend on the graphitic carbon−water interaction. Werder et al.[6] found that, by varying the carbon−water interaction, the predicted water contact angles on graphite can range from 138.8° to 50.7°. Similarly, Hummer et al.[5,9] showed that a small change in carbon−water interaction can lead to totally different predications of whether a CNT can be filled by water.

Various carbon−water interaction parameters have been proposed in the literature.[5,6,10−14] The carbon−water interactions are all based on a pair-additive Lennard-Jones (LJ) potential between the atoms of water and the carbon atoms. The functional form of the potential is $V_{ij}^{6\text{-}12} = 4\varepsilon[(\sigma/R_{ij})^{12} - (\sigma/R_{ij})^{6}]$, where R_{ij} is the separation distance between a pair of atoms of water and carbon atoms, ε is the depth of the potential well, and $2^{1/6}\sigma$ is the position of the potential well. The interaction parameter values available in the literature and the way they are obtained are summarized in Table 1. From Table 1, it can be seen that the current carbon−water interaction parameters either are developed by applying Lorentz−Berthelot combination rules[5,10−12,14] or are based on limited experimental data.[6,13,14]

Recently various force fields were developed based on data from first principles. Bukowski et al.[15] developed a force field for water entirely from first principles, without any fitting to experimental data. The force field was able to predict the spectra, second-virial coefficient of dimer, radial distribution function, internal energy, self-diffusion coefficient, and coordination number of liquid water. Pascal et al.[16] developed a quantum mechanics based force field at the M06-2X level and accurately predicted experimental lattice vibrations, elastic constant, Poisson ratios, lattice modes, phonon dispersion curves, specific heat, and thermal expansion of graphite. Chiu et al.[17] improved the 43A1 lipid force field using electronic structure computations and reproduced the experimental X-ray form factors and NMR order parameters over a wide range of membrane compositions. These studies based on first-principle calculations provide a way of obtaining the graphitic carbon−water interaction force field.

Pertsin et al.[18] made the first attempt to develop graphitic carbon−water interaction parameters from first-principle data. The ab initio data used were the graphene−water binding energy and lowest-energy geometry obtained by Feller et al.[19] The binding energy used was 5.8 kcal/mol, which is now

Received: February 27, 2013
Revised: May 29, 2013
Published: June 26, 2013

   dx.doi.org/10.1021/jp402051t | J. Phys. Chem. B 2013, 117, 8802−8813

Table 1. Summary of LJ Parameters in the Literature and from This Work, with Corresponding Graphene−Water Binding Energy E_b, Predicted Water Contact Angle θ on the Graphite Surface, and CNT RBM Frequency Shift Δf_{RBM}[a]

ref	carbon−water model	σ_{C-OW}	ε_{C-OW}	σ_{C-HW}	ε_{C-HW}	E_b	θ	Δf_{RBM}
Hummer et al.[5]	combine C−C from AMBER[44] and O−O from TIP3P[75]	3.275	0.1143	N/A	N/A	1.81	33.9	6.1
Won et al.[10]	combine C−C from Chen et al.[89] and O−O from SPC/E[48]	3.2779	0.1037	N/A	N/A	1.66	69.1	5.2
Noon et al.[11]	combine C−C from CHARMM[43] and O−O, H−H from modified TIP3P[65]	3.296	0.1382	2.58	0.0772	3.60	0.0	15.0
Gordillo et al.[12]	combine C−C, H−H from Steele et al.[90] and O−O from SPC-F2[91]	3.280	0.0930	2.81	0.0308	2.13	43.5	7.6
Werder et al.[6]	fits to an exptl water contact angle on graphite of 86°[77]	3.190	0.0937	N/A	N/A	1.43	86.9	4.2
Werder et al.[6]	fits to an exptl water contact angle on graphite of 42°[81]	3.190	0.1349	N/A	N/A	2.05	41.5	7.6
Scocchi[13]	fits to an exptl water contact angle on graphene of 127°[79]	3.190	0.0478	N/A	N/A	0.73	129.9	1.0
Markovic et al.[14]	C−OW by exptl oxygen gas adsptn on graphite,[92] C−HW by combining C−C, H−H from Steele et al.[90,93]	3.190	0.0935	2.82	0.0605	2.76	0.0	11.6
this work	fitting to MP2 data	3.430	0.1164	2.685	0.0263	2.54	10.3	8.8
this work	fitting to DFT-SAPT data[25]	3.372	0.1039	2.640	0.0256	2.24	34.2	8.2
this work	fitting to RPA data[24]	3.436	0.0850	2.690	0.0383	2.26	42.4	7.1
this work	fitting to CCSD(T) data[28]	3.126	0.1646	2.447	0.0246	2.84	<10	11.8

[a]The LJ parameters include the carbon−water oxygen parameters σ_{C-OW} and ε_{C-OW}, and the carbon−water hydrogen parameters σ_{C-HW} and ε_{C-HW}. σ_{C-OW} and σ_{C-HW} are in Å, ε_{C-OW} and ε_{C-HW} are in kcal/mol, E_b is in kcal/mol, θ is in deg, and Δf_{RBM} is in cm^{-1}. The error bar for each contact angle value is 3.6°. The error bar for the CNT RBM frequency shift is 0.6 cm^{-1}. The experimental value is 42 ± 7° for the water contact angle on the graphite surface,[81,82] and 7.3 cm^{-1} for the CNT RBM frequency shift.[86]

considered to be an overestimated value. The potential well depths were rescaled later[20] to obtain the graphene−water binding energy of 2.5 kcal/mol using a many-body polarizable model.[21] In both models, the potential well depth between water oxygen and carbon is smaller than that between water hydrogen and carbon, while generally it is considered that the oxygen−carbon interaction should be stronger than the hydrogen−carbon interaction. A higher-order dependence of R_{ij}^{-8} or R_{ij}^{-10} was used for the dispersion term, which physically should depend on R_{ij} to the power of 6. Also, parameter fittings were based on a trial-and-error procedure, and the parameters determined may not be optimal.

Recently, graphene−water interaction energies have been computed using various methods, including Møller−Plesset perturbation theory of the second order (MP2),[22,23] random-phase approximation (RPA),[24] diffusion Monte Carlo (DMC),[24] density functional theory-symmetry-adapted perturbation theory (DFT-SAPT),[25] density functional theory/coupled cluster (DFT/CC),[26] density functional theory with dispersion correction (DFT-D),[27] and coupled cluster treatment with single and double excitations and perturbative triples (CCSD(T)).[28] More than one orientation of the water molecule, with respect to the graphene plane, was considered. Also, the interaction energies at different separation distances between graphene and water were computed. This provides an opportunity to develop graphitic carbon−water interaction parameters entirely and uniquely from these ab initio data. Yet the development of graphitic carbon−water parameters using these ab initio data has not been attempted.

Møller−Plesset perturbation theory of the second order (MP2) method has been shown to be adequate to capture intermolecular binding energies for small molecules.[19] This method was used by Sudiarta et al.[22] and Cabaleiro-Lago[23] to compute the graphene−water interaction energy. The results of Sudiarta et al.[22] were questioned[29] due to the use of a small basis set (6-31G(d = 0.25)), which is inadequate to describe polarization and dispersion interactions. Cabaleiro-Lago[23] extrapolated the graphene−water interaction energies based on the energies obtained for polycyclic aromatic hydrocarbons (with the number of carbons considered less than or equal to 54) by assuming an exponential decay. It has been shown[22,25] that due to the long-range electrostatic multipole interaction, the convergence of the interaction energy for a cluster of 54 carbons is not adequate for an exponential decay. Proper decomposition of the interaction energy has to be done before the extrapolation.

In this work, we revisit the MP2 calculations of graphene−water interaction energies. A proper basis set is chosen, and the convergence of the interaction energies is verified. Then, we use the MP2 data from this work and the ab initio data from RPA,[24] DFT-SAPT,[25] and CCSD(T)[28] to develop graphitic carbon−water interaction parameters. The accuracy of the interaction parameters is checked by predicting properties, that is, water contact angle on graphite and CNT radial breathing mode (RBM) frequency shift due to surrounding water environment, and comparing them with experimental data. Both properties have been shown to depend on the graphitic carbon−water interaction parameters.[6,30] The rest of the paper is organized as follows: The next section describes the system configurations, ab initio methods, potential fitting, and the procedure to compute contact angle and CNT RBM frequency in MD. Then, the results of MP2 calculations, potential fitting, and comparison with experiments are discussed. The last section summarizes the paper.

METHODS

System Configurations Considered in Ab Initio Calculations. The infinite graphene is represented by the extrapolation of a series of increasing-size polycyclic aromatic hydrocarbon (PAH) clusters, as shown in Figure 1a−e. The C−C bond length and C−C−C bond angle (1.42 Å and 120°) in all clusters follow the experimental values for graphite.[31] The dangling bonds at the edge are terminated by hydrogen atoms, with C−H bond length of 1.09 Å and C−C−H bond angle of 120°. The water monomer follows the experimental gas phase geometry, with O−H bond length of 0.9572 Å and H−O−H angle of 104.52°.[32] Three water orientations with respect to

dx.doi.org/10.1021/jp402051t | J. Phys. Chem. B 2013, 117, 8802−8813

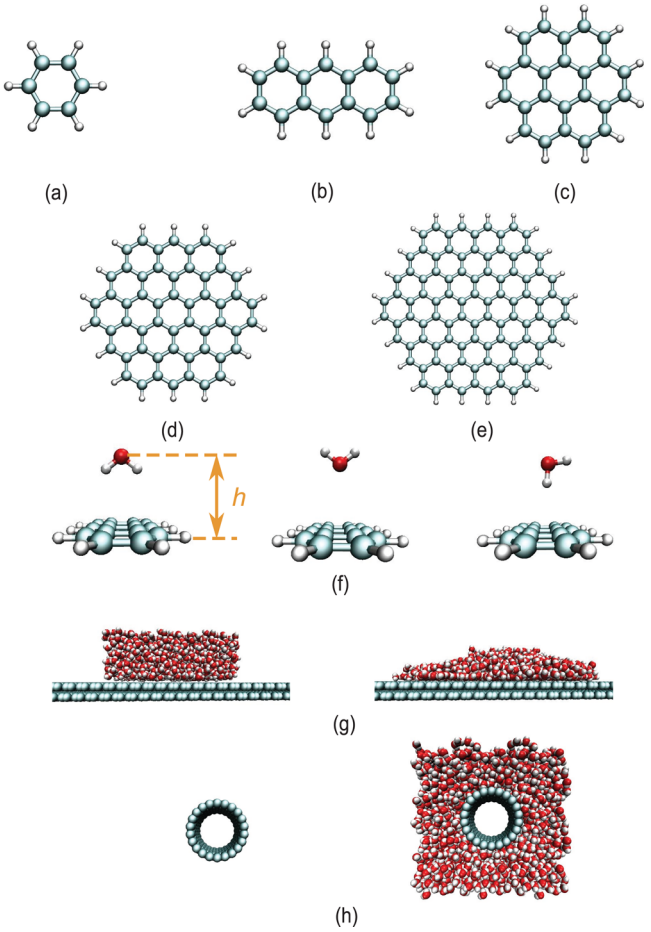

Figure 1. (a–e) PAH considered in ab initio calculations. (a) C_6H_6, benzene; (b) $C_{14}H_{10}$, anthracene; (c) $C_{24}H_{12}$, coronene; (d) $C_{54}H_{18}$, circumcoronene; (e) $C_{96}H_{24}$, dicircumcoronene. (f) Three water configurations with respect to PAH considered in ab initio calculations. From left to right: downward, upward, and pointing. Detailed description of each configuration can be found in the Methods section. The distance between water oxygen and the PAH plane is defined as *h*. (g) Contact angle measurement using MD. Left: initial configuration; right: water configuration after equilibration. (h) CNT radial breathing mode frequency measurement using MD. Left: CNT alone; right: CNT surrounded by water.

PAH clusters are considered: (a) Downward orientation: the water molecule is located above the center of the PAH cluster, with two hydrogens pointing to the PAH and dipole perpendicular to the PAH molecular plane, as shown in Figure 1f. (b) Upward orientation: the water molecule is located above the center of the PAH cluster, with two hydrogens pointing away from the PAH and dipole perpendicular to the PAH molecular plane, as shown in Figure 1f. (c) Pointing orientation: one O–H bond is pointing toward one carbon atom of the PAH cluster, and the other O–H bond is almost parallel to the PAH plane,[24] as shown in Figure 1f. The distance between water oxygen and the PAH plane is defined as *h*.

Ab Initio Calculations. The interaction energies between the PAH cluster and water are calculated by

$$\Delta E = E_{\mathrm{PAH-water}} - E_{\mathrm{PAH}} - E_{\mathrm{water}} \tag{1}$$

where $E_{\mathrm{PAH-water}}$, E_{PAH}, and E_{water} are the energies of the PAH cluster and the water dimer, the PAH cluster monomer, and the water monomer, respectively. The energies are computed by the MP2 method. The spin-component-scaled (SCS) technique, where the same-spin (ss) and opposite-spin (os) contributions to the correction energy are scaled by different factors, is used to correct the overestimation of the binding energy obtained from the standard MP2 method. The factors of $C_{ss} = 1.76$ and $C_{os} = 0$ by Hill and Platts[33] give the minimum mean absolute deviation for S22 test sets of noncovalently bonded dimers[34] and thus are used here. The counterpoise method[35] is utilized to eliminate the basis set superposition error.

The choice of method and basis set is validated by the CCSD(T) method with a complete basis set (CBS):[34,36]

$$\Delta E^{\mathrm{CCSD(T)/CBS}} = \Delta E^{\mathrm{MP2/CBS}} + (\Delta E^{\mathrm{CCSD(T)}} - \Delta E^{\mathrm{MP2}})_{\mathrm{small\ basis}}$$
$$\Delta E^{\mathrm{MP2/CBS}} = E^{\mathrm{HF}}_{\mathrm{CBS}} + E^{\mathrm{corr}}_{\mathrm{CBS}} \tag{2}$$

where $\Delta E^{\mathrm{CCSD(T)/CBS}}$ and $\Delta E^{\mathrm{MP2/CBS}}$ are the interaction energy evaluated using CCSD(T) and MP2 with a complete basis set, $(\Delta E^{\mathrm{CCSD(T)}} - \Delta E^{\mathrm{MP2}})_{\mathrm{small\ basis}}$ is the difference of the interaction energies evaluated using CCSD(T) and MP2 with a small basis set, E^{HF} and E^{corr} are the Hartree–Fock and second order correction components of the standard MP2 calculations, and $E^{\mathrm{HF}}_{\mathrm{CBS}}$ and $E^{\mathrm{corr}}_{\mathrm{CBS}}$ are the CBS extrapolation based on $E^{\mathrm{HF}}_X = E^{\mathrm{HF}}_{\mathrm{CBS}} + A\exp(-1.63X)$ and $E^{\mathrm{corr}}_X = E^{\mathrm{corr}}_{\mathrm{CBS}} + BX^{-3}$ using Dunning's correlation consistent basis set aug-cc-pVXZ (X = T,Q).[37] The small basis set used in eq 2 is 6-31G(d = 0.25).[38]

All MP2 and CCSD(T) calculations are done using Gaussian.[39]

Function Forms Considered in Potential Fitting. The general LJ*m-n* potential form to describe van der Waals (vdW) interaction between atoms is given by

$$V_{ij}^{m\text{-}n} = \frac{D_v}{n-m}\left[m\left(\frac{R_v}{R_{ij}}\right)^n - n\left(\frac{R_v}{R_{ij}}\right)^m\right] = \frac{C_n}{R_{ij}^n} - \frac{C_m}{R_{ij}^m}$$
$$(m = 6,\ n > m) \tag{3}$$

where D_v and R_v are the well depth and position, and R_{ij} is the separation distance between atom *i* and atom *j*. The force constant at the well position is $k_v = (\delta^2 E)/(\delta R^2)|_{R_v} = mn(D_v)/(R_v^2)$. Here *m* is equal to 6 because the dispersion and induction energy vary as R_{ij}^{-6}.[22] The general LJ*m-n* potential form is reduced to the commonly used LJ6-12 form when $n = 12$:

$$V_{ij}^{6\text{-}12} = D_v\left[\left(\frac{R_v}{R_{ij}}\right)^{12} - 2\left(\frac{R_v}{R_{ij}}\right)^6\right] = 4\varepsilon\left[\left(\frac{\sigma}{R_{ij}}\right)^{12} - \left(\frac{\sigma}{R_{ij}}\right)^6\right] \tag{4}$$

where $\varepsilon = D_v$ and $\sigma = (R_v/2^{1/6})$. Compared to the Buckingham and Morse potentials, which have a third parameter[16] to control the force constant k_v, the LJ*m-n* potential form has a fixed force constant once *m* and *n* are chosen. To study the effects of varying the force constant, the LJ6-14 function form[18,20] and the LJ6-10 potential form[40–42] are used besides the commonly used LJ6-12 potential form.[43–47]

Contact Angle Measurement Using MD Simulations. The contact angles of water droplets on a graphite surface are measured by MD simulations. The configurations of the systems are shown in Figure 1g. The graphite surface is represented by two staggered hexagonal carbon sheets with an interlayer distance of 3.4 Å. The dimension of each carbon layer

dx.doi.org/10.1021/jp402051t | J. Phys. Chem. B 2013, 117, 8802–8813

Table 2. Interaction Energies between PAH and Water[a]

ref	C_6H_6	$C_{14}H_{10}$	$C_{24}H_{12}$	$C_{54}H_{18}$	$C_{96}H_{24}$	graphene	approach
this work	−3.24	−3.18					CCSD(T)/CBS[b]
this work	−3.06	−3.05	−3.22	−3.11	−3.05	−2.51	MP2/6-311+G(3d,3p)
Lago et al.[23]	−2.72	−3.11	−3.15	−3.05		−2.50[c]	SCS-MP2/pVTZ[d]
Rubes et al.[26]	−3.15		−3.54	−3.51		−3.18	DFT/CC(aVQZ)[e]
Jenness et al.[25]	−3.16		−3.05	−2.93		−2.27[f]	DFT-SAPT/aVTZ[g]
Sudiarta et al.[22]	−2.55		−2.81	−2.80		−2.39	MP2/6-31G(d = 0.25)
Voloshina et al.[28]						−2.84	CCSD(T)/pVDZ
Ma et al.[24]						−2.26	RPA[h]
Ma et al.[24]						−1.44	DMC[i]

[a]All energies are in kcal/mol. The water molecule is located above the center of the PAH cluster, with two hydrogens pointing to the PAH and the dipole perpendicular to the PAH molecular plane. The water oxygen atom is 3.36 Å from the PAH plane. [b]CCSD(T) with complete basis set (CBS). [c]The value is corrected from the original −3.098 kcal/mol[23] by excluding the electrostatic multipole interaction before extrapolation. [d]Spin-component-scaled MP2 (SCS-MP2). [e]Density-functional/coupled-cluster (DFT/CC) theory. [f]The value is obtained from the original −3.18 kcal/mol[25] by considering that the graphene carbon quadrupole−water interaction is negligible.[22] [g]DFT based symmetry-adapted perturbation theory (DFT-SAPT). [h]Random-phase approximation (RPA). [i]Diffusion Monte Carlo (DMC).

is 20 nm × 20 nm, or 30 nm × 30 nm, depending on the droplet size to effectively remove the interaction between the droplet and its periodic images. The graphite surface is fixed throughout the simulation. The effects of fixing surface atoms on contact angle measurements are known to be negligible.[6] The water molecules are modeled by the SPC/E model.[48] The SPC/E water model has been used successfully in simulating water behavior in confined systems.[49] The SETTLE[50] or SHAKE constraint algorithm[51] is used to maintain the water geometry. The choice of constraint algorithms is found to have no effect on the predicted contact angle. The interactions between graphite atoms and water molecules use the developed LJ parameters. LJ6-10 and LJ6-14 function forms are implemented in GROMACS using lookup tables. The simulation box size perpendicular to the graphite surface plane is 20 nm. MD simulations are performed with the GROMACS 4.5.3 package.[52] Time integration is performed using the leapfrog algorithm[53] with a time step of 2.0 fs. The short-range vdW interactions are computed using a cutoff scheme (cutoff distance, 1.4 nm). The long-range electrostatic interactions are computed by using a particle mesh Ewald method[52] (real space cutoff, 1.4 nm; FFT grid spacing, 0.12 nm; fourth-order interpolation). The Nosé−Hoover thermostat[54,55] with a time constant of 0.5 ps is used to maintain the temperature at 300 K. A water cubic box is initially placed on top of the graphite surface. Different numbers of water molecules, i.e. 2000, 4000, and 8000, are considered to study the water droplet size effects. Each simulation is equilibrated for 6 ns using the NVT ensemble, during which the water cubic box evolves into a spherical shape. The energy and temperature of the simulation box reach constant values during this equilibration process. The resulting configuration is used as the starting point for further simulations. For collecting sufficient statistics to compute contact angles, the simulations are run for 6 ns.

CNT RBM Frequency Measurement Using MD Simulations. The RBM frequencies of an isolated CNT and a CNT surrounded by water are computed by MD simulations. The configurations of the systems are shown in Figure 1h. The adaptive intermolecular reactive empirical bond order (AIREBO) potential[56] is used to model the full dynamics of CNT. The water molecules are modeled by the SPC/E water model.[48] The interactions between CNT atoms and water molecules use the LJ parameters proposed in this work. The CNT considered in this work is a (22,0) zigzag tube, consisting of 352 carbon atoms. The CNT is replicated by periodic boundary conditions along the axial direction to represent an infinite tube. MD simulations are performed with the LAMMPS package.[57] Time integration is performed using the Verlet algorithm[58] with a time step of 0.5 fs. The short-range vdW interactions are computed using a cutoff scheme (cutoff distance, 1.2 nm). The long-range electrostatic interactions are computed by using a particle−particle particle-mesh algorithm. The Nosé−Hoover thermostat[54,55] with a time constant of 0.5 ps is used to maintain the temperature at 300 K. The CNT is first relaxed using the NPT ensemble for 200 ps. The pressure is maintained at 1 bar using the Parrinello−Rahman scheme.[59] Then the simulation is switched to the NVT ensemble to collect data for 500 ps. The position and velocity of each carbon atom are stored every 5 fs. The RBM frequency of CNT is calculated as follows:[30,60] first, velocities of carbon atoms are projected to the radial direction and averaged over all carbon atoms to obtain the average radial velocity of CNT, v_r, for each time frame. Second, the autocorrelation of the average radial velocity, $C(t)$, is computed by

$$C(t) = \frac{\langle v_r(t)\, v_r(0)\rangle}{\langle v_r(0)\, v_r(0)\rangle} \tag{5}$$

where $v_r(0)$ and $v_r(t)$ are the average radial velocity of CNT at time 0 and at time t. $\langle\rangle$ denotes average over 200 runs with different initial velocity profiles. Fourier transformation of the velocity autocorrelation gives the power spectra density, $S(\omega)$:

$$S(\omega) = \int_0^\infty \mathrm{d}t\; C(t)\cos \omega t \tag{6}$$

where $\omega = 2\pi f$ and f is the discrete frequency index. The RBM frequency of CNT corresponds to the peak position in the power spectra density. The least-squares fitting of a Gaussian function to the peak is done to obtain the frequency.

RESULTS AND DISCUSSION

MP2 and CCSD(T) Interaction Energies between PAH and a Water Molecule. The interaction energies for C_6H_6−water and $C_{14}H_{10}$−water systems for a separation distance of 3.36 Å with the downward water orientation are computed as −3.06 and −3.05 kcal/mol by MP2/6-311+G(3d,3p), compared to −3.24 and −3.18 kcal/mol by the CCSD(T)/CBS method. This shows that the MP2/6-311+G(3d,3p)

dx.doi.org/10.1021/jp402051t | J. Phys. Chem. B 2013, 117, 8802−8813

method can give a good estimate of the interaction between PAH and water with accuracy comparable to the CCSD(T) method. So MP2/6-311+G(3d,3p) is used to compute interaction energies on larger clusters: $C_{24}H_{12}$, $C_{54}H_{18}$, and $C_{96}H_{24}$.

The values computed in this work and their comparison to values reported in the literature are summarized in Table 2. The interaction energies computed by MP2/6-311+G(3d,3p) agree with those reported by Cabaleiro-Lago et al.[23] using the MP2/pVTZ method and compare well with those reported using other methods in the literature.

MP2 Interaction Energy Decomposition and Extrapolation. Before extrapolating the interaction energies between PAH and water to the infinite graphene limit, the effects of the PAH cluster boundary have to be considered: the C−H dipole created by termination hydrogen atoms contributes to the electrostatic interaction between PAH and water. So the total interaction energy is decomposed into the following components[22,25]

$$\Delta E = \Delta E_{ES} + \Delta E_{R} + \Delta E_{CORR} + \Delta E_{I} \quad (7)$$

where ΔE_{ES}, ΔE_{R}, ΔE_{CORR}, and ΔE_{I} are the electrostatic, repulsion, correlation, and induction energy components, respectively. The electrostatic energy component can be further decomposed into contributions from charge penetration[61] and from interactions between atom-centered multipole moments.[25] The electrostatic energy component between multipole moments of PAH and water is long-ranged, and it includes the extra electrostatic interaction mentioned above. Since the electrostatic energy component between multipole moments of graphene and water is negligible,[22] the electrostatic energy component between multipole moments of PAH and water is subtracted from the total interaction energy before the extrapolation is done.

The atomic charges, dipoles, and quadrupoles on each PAH atom are computed using Stone's Gaussian distributed multipole analysis (GDMA) tool[62] based on MP2/cc-pVDZ charge densities. The small basis set cc-pVDZ is used here since the calculated multipole moments by GDMA converge rapidly to stable values at small basis sets.[25,62] The contribution from the electron moments higher than quadrupole is negligible and thus not considered in the multipole analysis. The three point charges from the Dang-Chang model[63] are used to represent the electron moments of water. The use of the Dang-Chang model was well justified by comparing to distributed multipole analysis results.[25] The computed electrostatic multipole energy components for different PAH−water dimers are summarized in Table 3. These values agree with those reported by Jenness et al.[25]

Table 3. Electrostatic Multipole Component Is Subtracted from the Total Interaction Energy before Extrapolation[a]

	C_6H_6	$C_{24}H_{12}$	$C_{54}H_{18}$	$C_{96}H_{24}$	graphene
total interaction energy	−3.06	−3.22	−3.11	−3.05	−2.51
electrostatic multipole component	−1.80	−1.11	−0.71	−0.57	0.00
remaining energy component	−1.26	−2.12	−2.40	−2.48	−2.51

[a]All the energies are in kcal/mol. The water molecule is located above the center of the PAH cluster, with two hydrogens pointing to the PAH and with the dipole perpendicular to the PAH molecular plane. The water oxygen atom is 3.36 Å from the PAH plane.

The electrostatic component due to charge penetration is short-ranged and converges when the cluster is larger than a $C_{24}H_{12}$ molecule. The repulsion component is also short-ranged, and it converges when the size of the cluster is larger than the $C_{54}H_{18}$ molecule.[25] The addition of the repulsion and charge-penetration electrostatic components can be represented by the (C_n/R_{ij}^n) term in eq 3. The induction energy represents the non-negligible polarization[64] of water and PAH when they approach each other. Both the induction and correlation components vary as $1/R^6$, where R is the separation distance between PAH atoms and water atoms.[22] The addition of the induction and correlation components can be represented by the $(-C_6/R_{ij}^6)$ term in eq 3. The C_n and C_6 coefficients are obtained by fitting to $C_{54}H_{18}$−water energy profiles. The interaction energy for clusters larger than $C_{54}H_{18}$ is then extrapolated using the obtained fitting parameters.

Potential Fitting. The interaction energy between graphene and water depends on water orientation. Voloshina et al.[28] found that the lowest interaction energy for the upward orientation is 0.35 kcal/mol higher than that for the downward orientation using CCSD(T)/pVDZ, while Rubeš et al.[26] reported a 1.10 kcal/mol energy difference using DFT/CC(aVQZ). Such water-orientation dependence can be included in the fitting potential by having nonzero carbon−water hydrogen interaction parameters $\varepsilon_{C\text{-}HW}$ and $\sigma_{C\text{-}HW}$. $\sigma_{C\text{-}OW}$ and $\sigma_{C\text{-}HW}$ are reduced to one fitting parameter α by $\sigma_{C\text{-}OW} = \alpha\sigma^0_{C\text{-}OW}$ and $\sigma_{C\text{-}HW} = \alpha\sigma^0_{C\text{-}HW}$. The initial guess of $\sigma^0_{C\text{-}OW}$ = 3.296 Å and $\sigma^0_{C\text{-}HW}$ = 2.584 Å is directly taken from Neria et al.[65] The ab initio data considered here include the data from the MP2/6-311+G(3d,3p) and the data from DFT-SAPT,[25] CCSD(T)/pVDZ,[28] and RPA[24] available in the literature. The MP2/6-311+G(3d,3p) data set includes the $C_{54}H_{18}$−water interaction energies for the downward orientation at a series of h, with the electrostatic multipole component excluded. The DFT-SAPT data set includes the $C_{42}H_{18}$−water interaction energies for the downward orientation at a series of h, with the electrostatic multipole component excluded.[25] Since spin-scaled-MP2 methods are only optimized close to the equilibrated geometries, the methods tend to predict energies having an appreciable difference compared to the CCSD/CBS method for configurations far away from the equilibrated geometry.[23] So the energy difference of 0.35 kcal/mol between the downward and upward orientations and the equilibrated separation distance of 3.06 Å for the upward orientation obtained from the CCSD(T) calculation[28] are included in the MP2 data series to capture the water-orientation-dependence effects. The same treatment is done for the DFT-SAPT data series as well. The CCSD data set consists of the graphene−water interaction energies at a series of h for the upward orientation, the binding energy of 2.84 kcal/mol, and an equilibrated separation distance of 3.2 Å for the downward orientation.[24] The RPA data set contains the graphene−water interaction energies at a series of h for both the downward and pointing orientations.[24] We did not do the fitting to the DMC data[24] since the DMC data have large error bars and are not converged on k-points.

The fitting is done using a nonlinear least-squares fitting technique using the trust-region-reflective algorithm in Matlab (2007a, The MathWorks, Natick, MA). The fitted parameters for each ab initio data point are summarized in Table 1. The functional form used is the LJ6-12 form. Figure 2 shows the ab initio data and the fitted curve on the same plot. All the interaction parameters based on ab initio data tend to predict stronger carbon−water interaction. The same trend has been

dx.doi.org/10.1021/jp402051t | J. Phys. Chem. B 2013, 117, 8802−8813

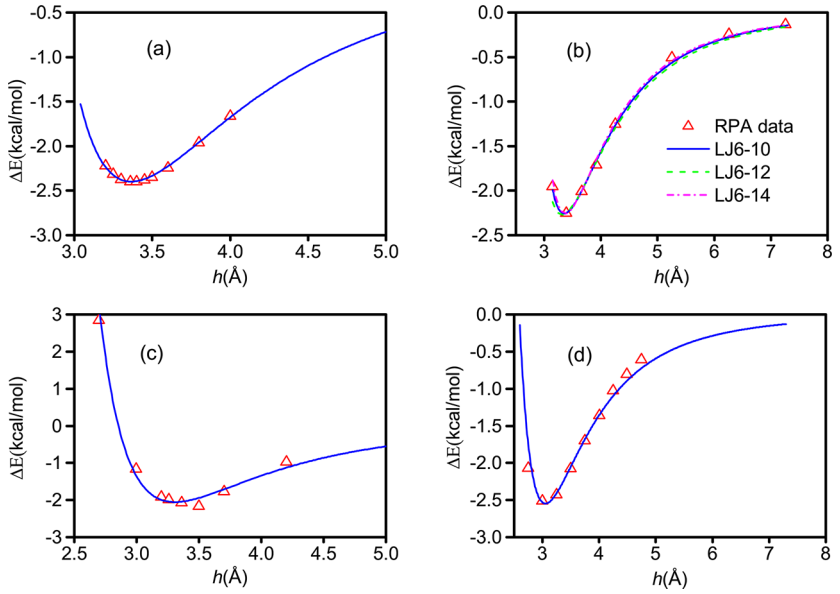

Figure 2. LJ functional forms fit to (a) MP2, (b) RPA, (c) DFT-SAPT, and (d) CCSD(T). The ab initio data are represented by triangles, and the LJ6-n fitting curves are represented by lines in each plot. h is the distance between the water oxygen and the PAH plane. In part b, three LJ6-n functional forms are fitted to the RPA data.

reported by DFT−Born−Oppenheimer MD simulation of water confined between graphene sheets and inside CNTs[66] and vdW density functional study of water−CNT systems.[67]

Three different function forms, namely LJ6-10, LJ6-12, and LJ6-14, are considered. These functions are fitted to the RPA ab initio data, as shown in Figure 2b. The resulting fitting parameters are summarized in Table 4. All the three functional forms give a good representation of the RPA ab initio data. The effect of various fitting functional forms will be further investigated by predicting contact angle using the three sets of parameters.

Table 4. Fitting to RPA ab Initio Data with Three LJ Function Forms Following Eq 3[a]

$m-n$	$R_{\nu C-OW}$	$D_{\nu C-OW}$	$R_{\nu C-HW}$	$D_{\nu C-HW}$
6−10	3.875	0.0633	3.033	0.0471
6−12	3.857	0.0850	3.019	0.0383
6−14	3.832	0.1056	2.999	0.0295

[a] $R_{\nu C-OW}$ and $D_{\nu C-OW}$ are the LJ parameters for carbon−water oxygen interactions, $R_{\nu C-HW}$ and $D_{\nu C-HW}$ are the LJ parameters for carbon−water hydrogen interactions. $R_{\nu C-OW}$ and $R_{\nu C-HW}$ are in nanometers, and $D_{\nu C-OW}$ and $D_{\nu C-HW}$ are in kilocalories/mole.

Graphene−Water Interaction Energy Calculated Using Fitted Parameters. Using the fitting parameters from the $C_{54}H_{18}$−water MP2 energy profile, the interaction energy between larger clusters and water can be extrapolated. The extrapolated interaction energy between $C_{96}H_{24}$ and water, with the electrostatic multipole component excluded, is −2.487 kcal/mol, compared to −2.478 kcal/mol computed by the MP2 and GDMA techniques. This confirms that the extrapolation based on the $C_{54}H_{18}$−water energy profile is capable of capturing larger cluster and water interactions. The graphene−water interaction is extrapolated as −2.51 kcal/mol, and this compares well with the literature values. Also the electrostatic multipole component between $C_{96}H_{24}$ and water is −0.57 kcal/mol, which is far from the converged value of close to zero for the graphene−water dimer. The electrostatic multipole component using only atomic quadropoles on carbon atoms is −0.29 kcal/mol for $C_{216}H_{36}$, and −0.14 kcal/mol for $C_{600}H_{60}$. So the energy decomposition for clusters smaller than $C_{96}H_{24}$ is necessary before extrapolation. If the same energy decomposition is done for the MP2 energy reported by Cabaleiro-Lago et al.,[23] the resulting graphene−water interaction energy is −2.50 kcal/mol, which agrees with the value from this work.

Contact Angle Calculations Using MD. Water contact angles on graphite surfaces are predicted using the carbon−water interaction parameters developed in this work and compared with experimental measurements. Various procedures[6,68−70] exist to measure contact angles using MD. It has been shown that the contact angle values measured by the nanodroplet procedure[6] agree with those by the cylindrical filament procedure[13] or by measuring individual surface tensions and computing contact angles using Young's equation.[70] We follow the most commonly used nanodroplet

Table 5. Contact Angles of Nanodroplets with Different Sizes and Macroscopic Droplet for Two Carbon−Water Interaction Parameters[a]

ref	σ_{C-OW}	ε_{C-OW}	σ_{C-HW}	ε_{C-HW}	$\theta_{nWt=2000}$	$\theta_{nWt=4000}$	$\theta_{nWt=8000}$	θ_∞	$\theta_{nWt=2000} - \theta_\infty$
Werder et al.[6]	3.190	0.0937	N/A	N/A	86.9 ± 0.3	85.5 ± 0.7	85.3 ± 0.3	82.6 ± 0.9	4.3 ± 1.0
this work, RPA	3.436	0.0850	2.690	0.0383	42.4 ± 1.0	40.9 ± 1.1	39.7 ± 1.5	36.4 ± 3.5	6.0 ± 3.6

[a] σ_{C-OW} and ε_{C-OW} are the LJ parameters for carbon−water oxygen interactions, and σ_{C-HW} and ε_{C-HW} are the LJ parameters for carbon−water hydrogen interactions. $\theta_{nWt=2000}$, $\theta_{nWt=4000}$, and $\theta_{nWt=8000}$ are the contact angles for nanodroplets composed of 2000, 4000, and 8000 water molecules, respectively. θ_∞ is the contact angle for a macroscopic droplet.

dx.doi.org/10.1021/jp402051t | J. Phys. Chem. B 2013, 117, 8802−8813

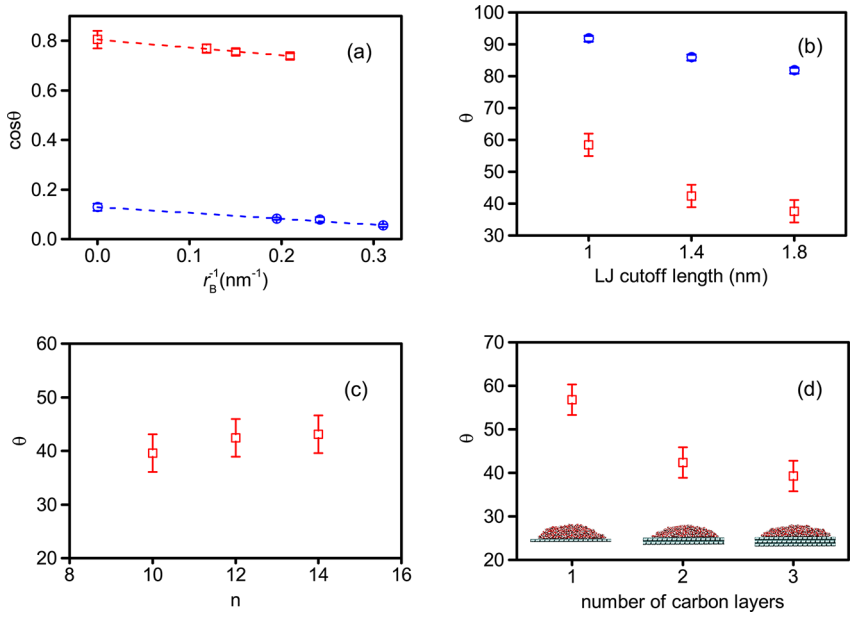

Figure 3. Water contact angles on clean graphite surface. (a) Extrapolation of nanodroplet contact angles θ to the macroscopic limit for carbon−water interaction parameters used by Werder et al.[6](represented by blue circles) and parameters obtained from RPA data (represented by red squares). (b) Dependence of contact angles on LJ cutoff length for the two carbon−water interaction parameters used in (a). (c) Dependence of contact angles on the choice of LJ6-*n* fitting function forms to the RPA data. The fitted parameters are summarized in Table 4. (d) Dependence of contact angles on the number of carbon layers. The contact angle values are in the unit of degrees. The contact angle values are the mean of three simulation runs with different initial velocity configurations. The error bar of the contact angle is 1.0° for the interaction parameters used by Werder et al.[6] and 3.6° for the RPA data.

procedure as outlined in Werder et al.[6] to compute the nanodroplet contact angles from the water density profile. Figure 1g shows the snapshot of one time frame of the equilibrated water droplet. 60,000 time frames are used to get the density profile of the equilibrated water droplet. The macroscopic contact angle θ_∞ is related to the nanodroplet contact angle θ (measured using MD) using the modified Young's equation,[71] $\cos\theta = \cos\theta_\infty - (\tau/\gamma_{LV})(1/r_B)$, where r_B is the radius of the contact area of water on graphite, τ is the line tension, and γ_{LV} is the surface energy of liquid water. Such dependence of contact angles on water droplet size has been verified recently by Scocchi et al.,[13] on condition that the number of water molecules forming the nanodroplet is larger than 2000. The extrapolation of the nanodroplet contact angles to obtain the macroscopic contact angle is checked for the carbon−water interaction parameters used by Werder et al.[6] and for the interaction parameters obtained from the RPA data. The contact angle values for nanodroplets with different sizes are summarized in Table 5. The mean and standard deviation of contact angles are obtained from three simulation runs with different initial velocity configurations. cos θ values are plotted against the reciprocal of r_B in Figure 3a. We note that, cos θ has a linear relation with $1/r_B$. The linear least-squares fitting is done to compute θ_∞, and the contact angle error bar associated with each nanodroplet size is propagated to θ_∞ following the procedure by Taylor.[72] The contact angle difference between the macroscopic droplet and the nanodroplet consisting of 2000 water molecules is 4.3 ± 1.0° for the parameters used by Werder et al.[6] and 6.0 ± 3.6° for the parameters obtained from the RPA ab initio data. From these results, we can infer that the contact angle value of a nanodroplet consisting of 2000 water molecules is a good representation of the macroscopic contact angle. Since this observation is valid for both carbon−water interaction parameter sets and for the contact angle ranges of 30−40° and 80−90°, we believe that this holds for other carbon−water interaction parameters considered in this work. In order to reduce the computational cost, except for the force fields obtained from the MP2 and CCSD(T) energies, we use the contact angle values of the droplet consisting of 2000 water molecules to represent the macroscopic contact angle. The same simplification has been used by Scocchi et al.[13] for graphene−water systems, by Zangi et al.[73] for graphite−water systems, and by Cruz-Chu et al.[74] for silica−water systems. For the force fields obtained from the MP2 and CCSD(T) energies, which predict contact angles less than 20°, droplets consisting of 16000 water molecules are used.

The dependence of contact angle on simulation parameters, e.g. LJ cutoff length, is studied. Sendner et al.[70] computed water contact angle on a carbon diamond-like surface by measuring individual surface tensions using MD, and LJ cutoff length was found to influence the contact angle, especially for small contact angles. The LJ cutoff length used was in the range of 0.8 to 1.4 nm. So the proper contact angle dependence on the LJ cutoff length has to be studied. Here we measure the contact angle of the droplet consisting of 2000 water molecules for the carbon−water interaction parameters used by Werder et al.[6] and obtained from the RPA ab initio data, using LJ cutoff lengths of 1.0, 1.4, and 1.8 nm. The resulting contact angle values are summarized in Figure 3b. The contact angle difference between the cutoff lengths of 1.4 and 1.8 nm is 3.3 ± 1.0° for parameters by Werder et al.[6] and 2.8 ± 3.6° for parameters obtained from the RPA data. For both cases, the difference is comparable to the error bar, implying that the contact angle is reasonably accurate for a cutoff length of 1.4 nm.

We also study various fitting function forms by considering three different functions, LJ6-10, LJ6-12, and LJ6-14. These functions are fitted to the RPA ab initio data. The resulting

dx.doi.org/10.1021/jp402051t | J. Phys. Chem. B 2013, 117, 8802−8813

fitting parameters are summarized in Table 4, and the corresponding contact angles in Figure 3c. We note that the function form does not influence the predicted contact angles as long as the fitted potential can represent the ab initio data well. Hence, the LJ6-12 function form is used since the LJ6-12 form is the function form that is commonly used in the literature for molecular dynamics simulations.

In the current study, two carbon layers are used to represent the graphite surface. We also investigate if adding extra carbon layers would affect the contact angle. For the interaction parameters obtained from the RPA ab initio data, we change the number of carbon layers from one to three, with everything else kept unchanged. The resulting contact angles are summarized in Figure 3d. The change in contact angle is negligible when the number of carbon layers is increased from two to three. But the monolayer graphene gives an appreciably larger contact angle than that of the double-layer graphite. Hence, we use two carbon layers as a good representation of the graphite surface.

The effects of different water models on the contact angle are also investigated. The SPC/E water model was found[6] to predict a 17.4° larger contact angle than the TIP3P[75] water model for the carbon–water interaction parameters used by Hummer et al.[5] We compute contact angles using the TIP5P water model[76] for the interaction parameters used by Werder et al.[6] The resulting contact angle is 82.8°, which compares well to 86.9° by the SPC/E water model with the same carbon–water interaction parameters. As a result, we use the SPC/E water model for all our contact angle simulations except for the interaction parameters used by Hummer et al.[5] The TIP3P water model is utilized for the interaction parameters used by Hummer et al., to be consistent with the work by Hummer et al.[5] The contact angles for all the carbon–water parameters are summarized in Table 1.

Comparing Predicted Contact Angles in MD with Experiments. The experimental water contact angles on a graphite surface available in the literature fall into two ranges: 80–90°, which is measured directly in air,[77−80] and 30–40°, which is measured using the ultrahigh vacuum technique.[81,82] In the latter work, Schrader[81] was able to reproduce the 80–90° if the experiments were done in air for the same graphite surface. Hydrocarbon contamination of the high-energy graphite surface from the air was suspected to be the cause of the high contact angle. MD simulations are done to confirm this by using ethane molecules as the hydrocarbon contamination. The force field for ethane molecules is taken from ref.83. Three contaminant surface coverage number densities of 0, 1.0, and 4.0 nm^{-2} are considered. Three carbon–water interaction parameters with varying graphene–water interaction strengths are used: the interaction parameters obtained from CCSD(T) data[28] have the strongest interaction strength (high-energy surface), the parameters used by Werder et al.[6] have the lowest interaction strength (low-energy surface), and the interaction parameters obtained from DFT-SAPT data[25] have the interaction strength in between. The contact angle of the water droplet on a clean surface is different from that on a contaminated surface, as shown in Figure 1g. The contact angles for each combination of carbon–water interaction parameters and contaminant surface coverage number densities are summarized in Figure 4. From Figure 4, the contact angles increase with increasing contaminant surface coverage density for all three carbon–water interaction parameters. The contact angles approach the same value when the surface coverage density is high, i.e. when the contaminants are closely packed on the surface and the water droplet is sitting on top of the contaminant. The influence of surface contamination on contact angle is more sensitive for a high-energy surface. These results suggest that, to simulate experimental contact angles measured in air, surface contamination has to be considered.

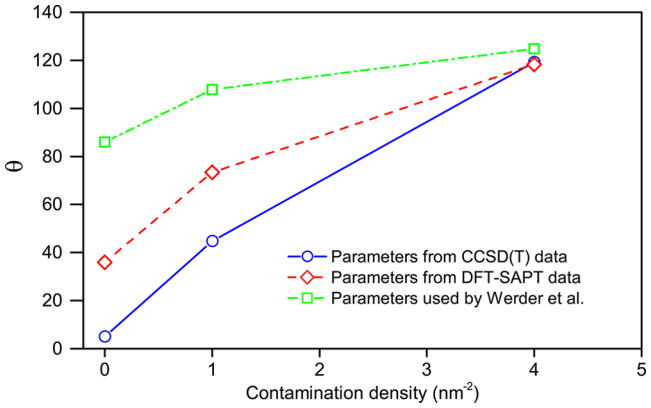

Figure 4. Effects of surface contamination on contact angle θ. Three graphitic carbon–water interaction parameters are considered: the interaction parameters used by Werder et al.,[6] the interaction parameters obtained from DFT-SAPT data, and the interaction parameters obtained from CCSD(T) data.

Next, we perform simulations on the clean surface and compare the contact angles to the experimental values[81,82] of 42 ± 7°. The contact angles predicted by the carbon–water interaction parameters obtained from the DFT-SAPT and RPA data agree pretty well with experiments. The carbon–water interaction parameters obtained from MP2 data slightly overestimate the carbon–water interaction strength. The interaction parameters obtained from CCSD(T) data tend to strongly overestimate the strength. Although the interaction parameters obtained from the DFT-SAPT and RPA data give a comparable graphene–water binding energy, the contact angles predicted by both methods deviate by around 8°. This shows that graphene–water binding energy alone may not be adequate in describing the graphitic carbon–water interaction. The dependence of graphene–water interaction energies on separation distance and orientation needs to be included in the development of graphitic carbon–water interaction parameters.

CNT RBM Frequency in MD and Comparison with Experiments. The RBM frequency of an isolated CNT, f_{RBM}, depends on the diameter of the CNT, d, by the formula[84] $f_{RBM} = C_1/d$, where the constant C_1 = 223.8 nm·cm^{-1} is obtained by comparing to Raman spectroscopy.[85] For a (22,0) CNT which has a diameter of 1.72 nm, the RBM frequency is 130.1 cm^{-1}. In MD, the AIREBO potential predicts the RBM frequency of a (22,0) CNT as 133.1 ± 0.3 cm^{-1}. The good agreement between MD and experimental data validates the AIREBO potential as a good model to study the RBM frequency of CNT.

When a CNT is immersed in water, due to the interaction between CNT carbon atoms and water molecules, the internal vibrational motion of the CNT changes. This change can be quantified by the shift in the RBM frequency of CNT, Δf_{RBM}, as shown in Figure 5. Longhurst and Quirke[30] showed that Δf_{RBM} depends sensitively on the carbon–water interaction parameters using MD. Experimentally Δf_{RBM} of a CNT immersed in water can be easily detected by modern Raman

dx.doi.org/10.1021/jp402051t | J. Phys. Chem. B 2013, 117, 8802–8813

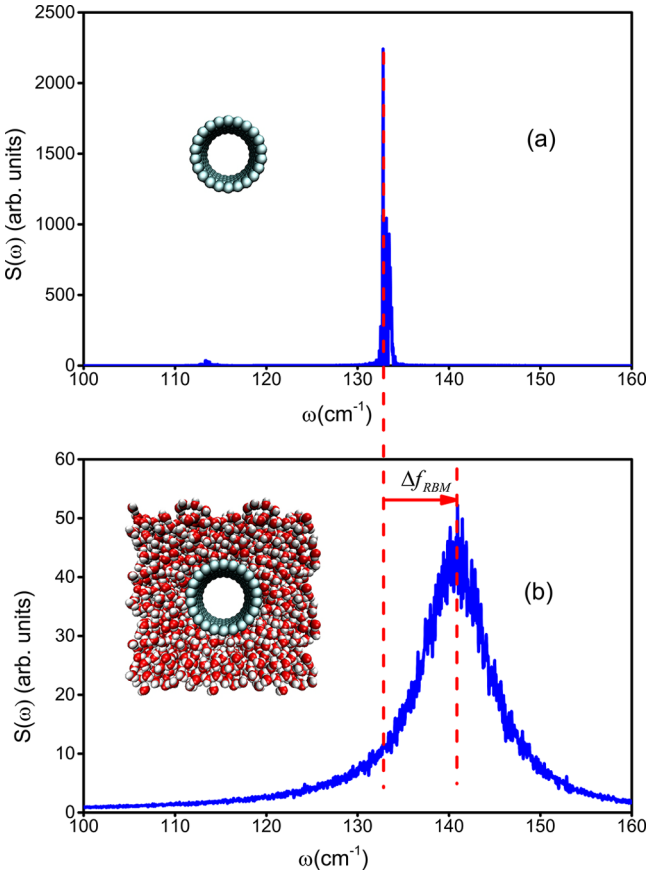

Figure 5. Power spectra obtained from MD for (a) an isolated (22,0) CNT and (b) a (22,0) CNT immersed in water. The peak in each figure corresponds to the radial breathing mode. The carbon−water interaction parameters obtained from DFT-SAPT data are used for part b.

machines, which provides an opportunity to probe the intermolecular forces between CNT and water. Using Raman spectroscopy, Izard et al.[86] measured a frequency shift of 7.3 cm^{-1} for (22,0) CNT. The carbon−water interaction parameters obtained from MP2 data predict a frequency shift of 8.8 ± 0.6 cm^{-1}, which agrees well with experiments. The RBM frequency of the (22,0) CNT immersed in water predicted by the carbon−water interaction parameters obtained from MP2 data is 141.9 ± 0.5 cm^{-1}, in agreement with the Raman spectroscopy measurement of 142.4 cm^{-1} for CNT in aqueous surfactant solutions.[87] The error of the CNT RBM frequency mainly comes from the Gaussian function fitting. A summary of Δf_{RBM} predicted by the carbon−water interaction parameters is listed in Table 1. The carbon−water interaction parameters obtained from RPA or DFT-SAPT data also predict a frequency shift that is in good agreement with experiments. The carbon−water interaction parameters obtained from CCSD(T) data overestimate the frequency shift probably due to the use of a small basis set in the CCSD(T) calculations.[28]

CONCLUSIONS

Graphitic carbon−water nonbonded interaction parameters are developed using ab initio calculation data. MP2 calculation of the PAH−water interaction energies is revisited, with proper consideration of the size of basis sets and energy component analysis to extrapolate to the infinite-sized graphene limit. Then graphitic carbon−water interaction parameters are fitted to MP2 data from this work and the ab initio data from RPA, DFT-SAPT, and CCSD(T) methods. The accuracy of the interaction parameters is evaluated by predicting water contact angle on graphite and CNT RBM frequency shift and comparing them with experimental data. The carbon−water interaction parameters obtained from MP2 data predict the CNT RBM frequency shift that is in good agreement with experiments. The carbon−water interaction parameters obtained from DFT-SAPT or RPA data predict both water contact angles and CNT RBM frequency shift that agree well with experiments. The carbon−water interaction parameters obtained from CCSD(T) data underestimate water contact angles and overestimate CNT RBM frequency shift probably due to the use of small basis sets in the CCSD(T) calculations.[28]

The good agreement of the predictions by the carbon−water interaction parameters obtained from DFT-SAPT and RPA data with experiments suggests that the graphitic carbon−water strength is stronger than previously thought. A recent scanning tunneling microscopy study[88] observed a monolayer of water trapped between graphene and CNT. Water does not experience capillary evaporation when confined between two graphitic carbon surfaces down to a monolayer thickness. This indicates a strong graphitic carbon−water interaction.

The carbon−water interaction parameters obtained from MP2, DFT-SAPT, and RPA data encapsulate the water orientation dependence by including the carbon−water hydrogen interaction. The inclusion of the water orientation dependence is important to describe water dynamics close to the surface. Here including the water orientation dependence based on ab initio data, not from the combinational rule, is a step forward.

More accurate DMC calculations are required to develop reliable carbon−water interaction parameters. All the ab initio data used in this work are interaction energies between a single water molecule and graphene. Multiple water molecules might interact differently with graphene. Ab initio calculations on multiple water molecules−graphene would be valuable for the development of carbon−water interaction parameters.

AUTHOR INFORMATION

Corresponding Author

*E-mail: aluru@illinois.edu.

Notes

The authors declare no competing financial interest.

ACKNOWLEDGMENTS

This work is supported by NSF under Grants 0328162 (nano-CEMMS, UIUC), 0852657, and 0915718. This work used the Extreme Science and Engineering Discovery Environment (XSEDE), which is supported by National Science Foundation Grant Number OCI-1053575.

REFERENCES

(1) Ghosh, S.; Sood, A. K.; Kumar, N. Carbon Nanotube Flow Sensors. *Science* **2003**, *299*, 1042−1044.

(2) Nguyen, C. V.; Delzeit, L.; Cassell, A. M.; Li, J.; Han, J.; Meyyappan, M. Preparation of Nucleic Ccid Functionalized Carbon Nanotube Arrays. *Nano Lett.* **2002**, *2*, 1079−1081.

(3) Holt, J. K.; Park, H. G.; Wang, Y. M.; Stadermann, M.; Artyukhin, A. B.; Grigoropoulos, C. P.; Noy, A.; Bakajin, O. Fast Mass Transport Through Sub-2-nanometer Carbon Nanotubes. *Science* **2006**, *312*, 1034−1037.

(4) Majumder, M.; Chopra, N.; Andrews, R.; Hinds, B. J. Nanoscale Hydrodynamics—Enhanced Flow in Carbon Nanotubes. *Nature* **2005**, *438*, 44−44.
(5) Hummer, G.; Rasaiah, J.; Noworyta, J. Water Conduction through the Hydrophobic Channel of a Carbon Nanotube. *Nature* **2001**, *414*, 188−190.
(6) Werder, T.; Walther, J.; Jaffe, R.; Halicioglu, T.; Koumoutsakos, P. On the Water-carbon Interaction for Use in Molecular Dynamics Simulations of Graphite and Carbon Nanotubes. *J. Phys. Chem. B* **2003**, *107*, 1345−1352.
(7) Joseph, S.; Aluru, N. R. Why Are Carbon Nanotubes Fast Transporters of Water? *Nano Lett.* **2008**, *8*, 452−458.
(8) Suk, M. E.; Aluru, N. R. Water Transport Through Ultrathin Graphene. *J. Phys. Chem. Lett.* **2010**, *1*, 1590−1594.
(9) Waghe, A.; Rasaiah, J.; Hummer, G. Filling and Emptying Kinetics of Carbon Nanotubes in Water. *J. Chem. Phys.* **2002**, *117*, 10789−10795.
(10) Won, C. Y.; Joseph, S.; Aluru, N. R. Effect of Quantum Partial Charges on the Structure and Dynamics of Water in Single-walled Carbon Nanotubes. *J. Chem. Phys.* **2006**, *125*, 114701.
(11) Noon, W. H.; Ausman, K. D.; Smalley, R. E.; Ma, J. P. Helical Ice-sheets inside Carbon Nanotubes in the Physiological Condition. *Chem. Phys. Lett.* **2002**, *355*, 445−448.
(12) Gordillo, M. C.; Martí, J. Hydrogen Bond Structure of Liquid Water Confined in Nanotubes. *Chem. Phys. Lett.* **2000**, *329*, 341−345.
(13) Scocchi, G.; Sergi, D.; D'Angelo, C.; Ortona, A. Wetting and Contact-line Effects for Spherical and Cylindrical Droplets on Graphene Layers: A Comparative Molecular-dynamics Investigation. *Phys. Rev. E* **2011**, *84*
(14) Marković, N.; Andersson, P. U.; Någård, M. B.; Pettersson, J. B. C. Scattering of Water from Graphite: Simulations and Experiments. *Chem. Phys.* **1999**, *247*, 413−430.
(15) Bukowski, R.; Szalewicz, K.; Groenenboom, G.; van der Avoird, A. Predictions of the Properties of Water from First Principles. *Science* **2007**, *315*, 1249.
(16) Pascal, T.; Karasawa, N.; Goddard, W., III. Quantum Mechanics Based Force Field for Carbon (QMFF-Cx) Validated to Reproduce the Mechanical and Thermodynamics Properties of Graphite. *J. Chem. Phys.* **2010**, *133*, 134114.
(17) Chiu, S.; Pandit, S.; Scott, H.; Jakobsson, E. An Improved United Atom Force Field for Simulation of Mixed Lipid Bilayers. *J. Phys. Chem. B* **2009**, *113*, 2748−2763.
(18) Pertsin, A.; Grunze, M. Water-graphite Interaction and Behavior of Water Near the Graphite Surface. *J. Phys. Chem. B* **2004**, *108*, 1357−1364.
(19) Feller, D.; Jordan, K. D. Estimating the Strength of the Water/Single-layer Graphite Interaction. *J. Phys. Chem. A* **2000**, *104*, 9971−9975.
(20) Pertsin, A.; Grunze, M. Water as a Lubricant for Graphite: A Computer Simulation Study. *J. Chem. Phys.* **2006**, *125*, 114707.
(21) Karapetian, K.; Jordan, K. D. In *Water in Confining Geometries*; Buch, V., Devlin, J. P., Eds.; Springer: Berlin, 2003; pp 139−150.
(22) Sudiarta, I. W.; Geldart, D. J. Interaction Energy of a Water Molecule with a Single-layer Graphitic Surface Modeled by Hydrogen- and Fluorine-terminated Clusters. *J. Phys. Chem. A* **2006**, *110*, 10501−6.
(23) Cabaleiro-Lago, E. M.; Carrazana-García, J. A.; Rodríguez-Otero, J. Study of the Interaction between Water and Hydrogen Sulfide with Polycyclic Aromatic Hydrocarbons. *J. Chem. Phys.* **2009**, *130*, 234307.
(24) Ma, J.; Michaelides, A.; Alfè, D.; Schimka, L.; Kresse, G.; Wang, E. Adsorption and Diffusion of Water on Graphene from First Principles. *Phys. Rev. B* **2011**, *84*033402
(25) Jenness, G. R.; Karalti, O.; Jordan, K. D. Benchmark Calculations of Water-acene Interaction Energies: Extrapolation to the Water-graphene Limit and Assessment of Dispersion-corrected DFT Methods. *Phys. Chem. Chem. Phys.* **2010**, *12*, 6375−81.
(26) Ruběs, M.; Nachtigall, P.; Vondrášek, J.; Bludský, O. Structure and Stability of the Water-graphite Complexes. *J. Phys. Chem. C* **2009**, *113*, 8412−8419.
(27) Li, H.; Zeng, X. C. Wetting and Interfacial Properties of Water Nanodroplets in Contact with Graphene and Monolayer Boron-nitride Sheets. *ACS Nano* **2012**, *6*, 2401−2409.
(28) Voloshina, E.; Usvyat, D.; Schütz, M.; Dedkov, Y.; Paulus, B. On the Physisorption of Water on Graphene: a CCSD(T) Study. *Phys. Chem. Chem. Phys.* **2011**, *13*, 12041−7.
(29) Jenness, G. R.; Jordan, K. D. DF-DFT-SAPT Investigation of the Interaction of a Water Molecule to Coronene and Dodecabenzocoronene: Implications for the Water-Graphite Interaction. *J. Phys. Chem. C* **2009**, *113*, 10242−10248.
(30) Longhurst, M.; Quirke, N. The Environmental Effect on the Radial Breathing Mode of Carbon Nanotubes. II. Shell Model Approximation for Internally and Externally Adsorbed Fluids. *J. Chem. Phys.* **2006**, *125*, 184705.
(31) Weast, R.; Astle, M.; Beyer, W. *CRC Handbook of Chemistry and Physics*; CRC Press: Boca Raton, FL, 1988; Vol. *69*
(32) Benedict, W. S.; Gailar, N.; Plyler, E. K. Rotation-vibration Spectra of Deuterated Water Vapor. *J. Chem. Phys.* **1956**, *24*, 1139−1165.
(33) Hill, J. G.; Platts, J. A. Spin-component Scaling Methods for Weak and Stacking Interactions. *J. Chem. Theory Comput.* **2007**, *3*, 80−85.
(34) Jurečka, P.; Šponer, J.; Černy, J.; Hobza, P. Benchmark Database of Accurate (MP2 and CCSD(T) Complete Basis Set Limit) Interaction Energies of Small Model Complexes, DNA Base Pairs, and Amino Acid Pairs. *Phys. Chem. Chem. Phys.* **2006**, *8*, 1985−93.
(35) Boys, S. F.; Bernardi, F. The Calculation of Small Molecular Interactions by the Differences of Separate Total Energies. Some Procedures with Reduced Errors. *Mol. Phys.* **1970**, *19*, 553−566.
(36) Halkier, A.; Helgaker, T.; Jørgensen, P.; Klopper, W.; Olsen, J. Basis-set Convergence of the Energy in Molecular Hartree-Fock Calculations. *Chem. Phys. Lett.* **1999**, *302*, 437−446.
(37) Kendall, R. A.; Dunning, T. H.; Harrison, R. J. Electron-affinities of the 1st-row Atoms Revisited - Systematic Basis-sets and Wave-functions. *J. Chem. Phys.* **1992**, *96*, 6796−6806.
(38) Jurečka, P.; Hobza, P. On the Convergence of the (dECCSD-(T)-dEMP2) Term for Complexes with Multiple H-bonds. *Chem. Phys. Lett.* **2002**, *365*, 89−94.
(39) Frisch, M. J.; Trucks, G. W.; Schlegel, H. B.; Scuseria, G. E.; Robb, M. A.; Cheeseman, J. R.; Montgomery, J. A., Jr.; Vreven, T.; Kudin, K. N.; Burant, J. C.; Millam, J. M.; Iyengar, S. S.; Tomasi, J.; Barone, V.; Mennucci, B.; Cossi, M.; Scalmani, G.; Rega, N.; Petersson, G. A.; Nakatsuji, H.; Hada, M.; Ehara, M.; Toyota, K.; Fukuda, R.; Hasegawa, J.; Ishida, M.; Nakajima, T.; Honda, Y.; Kitao, O.; Nakai, H.; Klene, M.; Li, X.; Knox, J. E.; Hratchian, H. P.; Cross, J. B.; Bakken, V.; Adamo, C.; Jaramillo, J.; Gomperts, R.; Stratmann, R. E.; Yazyev, O.; Austin, A. J.; Cammi, R.; Pomelli, C.; Ochterski, J. W.; Ayala, P. Y.; Morokuma, K.; Voth, G. A.; Salvador, P.; Dannenberg, J. J.; Zakrzewski, V. G.; Dapprich, S.; Daniels, A. D.; Strain, M. C.; Farkas, O.; Malick, D. K.; Rabuck, A. D.; Raghavachari, K.; Foresman, J. B.; Ortiz, J. V.; Cui, Q.; Baboul, A. G.; Clifford, S.; Cioslowski, J.; Stefanov, B. B.; Liu, G.; Liashenko, A.; Piskorz, P.; Komaromi, I.; Martin, R. L.; Fox, D. J.; Keith, T.; Al-Laham, M. A.; Peng, C. Y.; Nanayakkara, A.; Challacombe, M.; Gill, P. M. W.; Johnson, B.; Chen, W.; Wong, M. W.; Gonzalez, C.; Pople, J. A. *Gaussian 03*, revision C.02; Gaussian, Inc.: Wallingford, CT, 2004.
(40) Sun, H. COMPASS: An ab Initio Force-field Optimized for Condensed-phase Applications—Overview with Details on Alkane and Benzene Compounds. *J. Phys. Chem. B* **1998**, *102*, 7338−7364.
(41) Maple, J. R.; Dinur, U.; Hagler, A. T. Derivation of Force-fields for Molecular Mechanics and Dynamics from ab Initio Energy Surfaces. *Proc. Natl. Acad. Sci.* **1988**, *85*, 5350−5354.
(42) Heinz, H.; Vaia, R. A.; Farmer, B. L.; Naik, R. R. Accurate Simulation of Surfaces and Interfaces of Face-Centered Cubic Metals using 12−6 and 9−6 Lennard-Jones Potentials. *J. Phys. Chem. C* **2008**, *112*, 17281−17290.

(43) Brooks, B. R.; Bruccoleri, R. E.; Olafson, B. D.; States, D. J.; Swaminathan, S.; Karplus, M. CHARMM—A Program for Macromolecular Energy, Minimization, and Dynamics Calculations. *J. Comput. Chem.* **1983**, *4*, 187−217.
(44) Cornell, W. D.; Cieplak, P.; Bayly, C. I.; Gould, I. R.; Merz, K. M.; Ferguson, D. M.; Spellmeyer, D. C.; Fox, T.; Caldwell, J. W.; Kollman, P. A. A 2nd Generation Force-Field for the Simulation of Proteins, Nucleic-acids, and Organic-molecules. *J. Am. Chem. Soc.* **1995**, *117*, 5179−5197.
(45) Jorgensen, W. L.; Maxwell, D. S.; Tirado-Rives, J. Development and Testing of the OPLS All-atom Force Field on Conformational Energetics and Properties of Organic Liquids. *J. Am. Chem. Soc.* **1996**, *118*, 11225−11236.
(46) van Gunsteren, W.; Billeter, S.; Eising, A.; Hnenberger, P.; Krger, P.; Mark, A.; Scott, W.; Tironi, I. *The GROMOS Manual and User Guide*; vdf Hochschulverlag AG: Zürich, Switzerland, 1996.
(47) Wu, Y.; Joseph, S.; Aluru, N. R. Effect of Cross-linking on the Diffusion of Water, Ions, and Small Molecules in Hydrogels. *J. Phys. Chem. B* **2009**, *113*, 3512−20.
(48) Berendsen, H.; Grigera, J.; Straatsma, T. The Missing Term in Effective Pair Potentials. *J. Phys. Chem.* **1987**, *91*, 6269−6271.
(49) Chiu, S. W.; Subramaniam, S.; Jakobsson, E. Simulation Study of a Gramicidin/lipid Bilayer System in Excess Water and Lipid. I. Structure of the Molecular Complex. *Biophys. J.* **1999**, *76*, 1929−1938.
(50) Miyamoto, S.; Kollman, P. A. SETTLE—An Analytical Version of the SHAKE and RATTLE Algorithm for Rigid Water Models. *J. Comput. Chem.* **1992**, *13*, 952−962.
(51) Ryckaert, J.-P.; Ciccotti, G.; Berendsen, H. J. C. Numerical Integration of the Cartesian Equations of Motion of a System with Constraints: Molecular Dynamics of n-Alkanes. *J. Comput. Phys.* **1977**, *23*, 327−341.
(52) Lindahl, E.; Hess, B.; van der Spoel, D. GROMACS 3.0: A Package for Molecular Simulation and Trajectory Analysis. *J. Mol. Model.* **2001**, *7*, 306−317.
(53) Hockney, R. W.; Goel, S. P.; Eastwood, J. W. Quiet High-Resolution Computer Models of a Plasma. *J. Comput. Phys.* **1974**, *14*, 148−158.
(54) Nosé, S. A Molecular Dynamics Method for Simulations in the Canonical Ensemble. *Mol. Phys.* **2002**, *100*, 191−198.
(55) Hoover, W. G. Canonical Dynamics: Equilibrium Phase-space Distributions. *Phys. Rev. A* **1985**, *31*, 1695−1697.
(56) Stuart, S. J.; Tutein, A. B.; Harrison, J. A. A Reactive Potential for Hydrocarbons with Intermolecular Interactions. *J. Chem. Phys.* **2000**, *112*, 6472−6486.
(57) Plimpton, S. Fast Parallel Algorithms for Short-range Molecular-dynamics. *J. Comput. Phys.* **1995**, *117*, 1−19.
(58) Verlet, L. Computer Experiments on Classical Fluids. I. Thermodynamical Properties of Lennard-Jones Molecules. *Phys. Rev.* **1967**, *159*, 98−103.
(59) Parrinello, M.; Rahman, A. Polymorphic Transitions in Single Crystals: A New Molecular Dynamics Method. *J. Appl. Phys.* **1981**, *52*, 7182−7190.
(60) Longhurst, M.; Quirke, N. The Environmental Effect on the Radial Breathing Mode of Carbon Nanotubes in Water. *J. Chem. Phys.* **2006**, *124*, 234708.
(61) Kairys, V.; Jensen, J. H. Evaluation of the Charge Penetration Energy between Non-orthogonal Molecular Orbitals Using the Spherical Gaussian Overlap Approximation. *Chem. Phys. Lett.* **1999**, *315*, 140−144.
(62) Stone, A. J. Distributed Multipole Analysis: Stability for Large Basis Sets. *J. Chem. Theory Comput.* **2005**, *1*, 1128−1132.
(63) Dang, L. X.; Chang, T. M. Molecular Dynamics Study of Water Clusters, Liquid, and Liquid-vapor Interface of Water with Many-body Potentials. *J. Chem. Phys.* **1997**, *106*, 8149−8159.
(64) Schyman, P.; Jorgensen, W. L. Exploring Adsorption of Water and Ions on Carbon Surfaces Using a Polarizable Force Field. *J Phys. Chem. Lett.* **2013**, *4*, 468−474.
(65) Neria, E.; Fischer, S.; Karplus, M. Simulation of Activation Free Energies in Molecular Systems. *J. Chem. Phys.* **1996**, *105*, 1902−1921.
(66) Cicero, G.; Grossman, J. C.; Schwegler, E.; Gygi, F.; Galli, G. Water Confined in Nanotubes and between Graphene Sheets: A First Principle Study. *J. Am. Chem. Soc.* **2008**, *130*, 1871−8.
(67) Kaukonen, M.; Gulans, A.; Havu, P.; Kauppinen, E. Lennard-Jones Parameters for Small Diameter Carbon Nanotubes and Water for Molecular Mechanics Simulations from van der Waals Density Functional Calculations. *J. Comput. Chem.* **2012**, *33*, 652−658.
(68) Lundgren, M.; Allan, N. L.; Cosgrove, T.; George, N. Wetting of Water and Water/ethanol Droplets on a Non-polar Surface: A Molecular Dynamics Study. *Langmuir* **2002**, *18*, 10462−10466.
(69) Leroy, F.; Müller-Plathe, F. Solid-liquid Surface Free Energy of Lennard-Jones Liquid on Smooth and Rough Surfaces Computed by Molecular Dynamics using the Phantom-wall Method. *J. Chem. Phys.* **2010**, *133*, 044110.
(70) Sendner, C.; Horinek, D.; Bocquet, L.; Netz, R. R. Interfacial Water at Hydrophobic and Hydrophilic Surfaces: Slip, Viscosity, and Diffusion. *Langmuir* **2009**, *25*, 10768−10781.
(71) Wang, J. Y.; Betelu, S.; Law, B. M. Line Tension Approaching a First-Order Wetting Transition: Experimental Results from Contact Angle Measurements. *Phys. Rev. E* **2001**, *63*
(72) Taylor, J. *An Introduction to Error Analysis: the Study of Uncertainties in Physical Measurements*; University Science Books: 1997.
(73) Zangi, R.; Berne, B. J. Temperature Dependence of Dimerization and Dewetting of Large-Scale Hydrophobes: A Molecular Dynamics Study. *J. Phys. Chem. B* **2008**, *112*, 8634−8644.
(74) Cruz-Chu, E. R.; Aksimentiev, A.; Schulten, K. Water-silica Force Field for Simulating Nanodevices. *J. Phys. Chem. B* **2006**, *110*, 21497−21508.
(75) Jorgensen, W. L.; Chandrasekhar, J.; Madura, J. D.; Impey, R. W.; Klein, M. L. Comparison of Simple Potential Functions for Simulating Liquid Water. *J. Chem. Phys.* **1983**, *79*, 926−935.
(76) Mahoney, M. W.; Jorgensen, W. L. A Five-site Model for Liquid Water and the Reproduction of the Density Anomaly by Rigid, Nonpolarizable Potential Functions. *J. Chem. Phys.* **2000**, *112*, 8910.
(77) Fowkes, F.; Harkins, W. The State of Monolayers Adsorbed at the Interface Solid-aqueous Solution. *J. Am. Chem. Soc.* **1940**, *62*, 3377−3386.
(78) Morcos, I. On Contact Angle and Dispersion Energy of the Cleavage Graphite/water System. *J. Colloid Interface Sci.* **1970**, *34*, 469−471.
(79) Wang, S.; Zhang, Y.; Abidi, N.; Cabrales, L. Wettability and Surface Free Energy of Graphene Films. *Langmuir* **2009**, *25*, 11078−11081.
(80) Shin, Y.; Wang, Y.; Huang, H.; Kalon, G.; Wee, A.; Shen, Z.; Bhatia, C.; Yang, H. Surface-energy Engineering of Graphene. *Langmuir* **2010**, *26*, 3798−3802.
(81) Schrader, M. Ultrahigh Vacuum Techniques in the Measurement of Contact Angles. IV. Water on Graphite (0001). *J. Phys. Chem.* **1975**, *79*, 2508−2515.
(82) Schrader, M. Ultrahigh-vacuum Techniques in the Measurement of Contact Angles. 5. LEED Study of the Effect of Structure on the Wettability of Graphite. *J. Phys. Chem.* **1980**, *84*, 2774−2779.
(83) Siepmann, J. I.; Karaborni, S.; Smit, B. Simulating the Critical-behavior of Complex Fluids. *Nature* **1993**, *365*, 330−332.
(84) Jishi, R. A.; Venkataraman, L.; Dresselhaus, M. S.; Dresselhaus, G. Phonon Modes in Carbon Nanotubules. *Chem. Phys. Lett.* **1993**, *209*, 77−82.
(85) Bandow, S.; Asaka, S.; Saito, Y.; Rao, A. M.; Grigorian, L.; Richter, E.; Eklund, P. C. Effect of the Growth Temperature on the Diameter Distribution and Chirality of Single-wall Carbon Nanotubes. *Phys. Rev. Lett.* **1998**, *80*, 3779−3782.
(86) Izard, N.; Riehl, D.; Anglaret, E. Exfoliation of Single-wall Carbon Nanotubes in Aqueous Surfactant Suspensions: A Raman Study. *Phys. Rev. B* **2005**, *71*, 195417.
(87) Bachilo, S. M.; Strano, M. S.; Kittrell, C.; Hauge, R. H.; Smalley, R. E.; Weisman, R. B. Structure-assigned Optical Spectra of Single-walled Carbon Nanotubes. *Science* **2002**, *298*, 2361−2366.

(88) He, K. T.; Wood, J. D.; Doidge, G. P.; Pop, E.; Lyding, J. W. Scanning Tunneling Microscopy Study and Nanomanipulation of Graphene-coated Water on Mica. *Nano Lett.* **2012**, *12*, 2665−2672.
(89) Schluter, M.; Lannoo, M.; Needels, M.; Baraff, G.; Tomĺćnek, D. Electron-phonon Coupling and Superconductivity in Alkali-intercalated C60 Solid. *Phys. Rev. Lett.* **1992**, *68*, 526−529.
(90) Steele, W. *The Interaction of Gases with Solid Surfaces*; Pergamon Press: Oxford, U.K., 1974.
(91) Martí, J.; Guàrdia, E.; Padró, J. A. Dielectric-properties and Infrared-spectra of Liquid Water—Influence of the Dynamic Cross Correlations. *J. Chem. Phys.* **1994**, *101*, 10883−10891.
(92) Bojan, M. J.; Steele, W. A. Interactions of Diatomic Molecules with Graphite. *Langmuir* **1987**, *3*, 1123−1127.
(93) Cheng, A.; Steele, W. A. Computer-simulation of Ammonia on Graphite. I. Low-temperature Structure of Monolayer and Bilayer Films. *J. Chem. Phys.* **1990**, *92*, 3858−3866.